Author Manuscript

Author Manuscript

Author Manuscript

Author Manuscript

HHS Public Access

Author manuscript

Clin Cancer Res. Author manuscript; available in PMC 2017 May 15.

Published in final edited form as:

Clin Cancer Res. 2016 May 15; 22(10): 2351–2358. doi:10.1158/1078-0432.CCR-15-2013.

A novel crizotinib-resistant solvent-front mutation responsive to cabozantinib therapy in a patient with ROS1-rearranged lung cancer

Alexander Drilon[1,2,*], **Romel Somwar**[3], **Jacob. P. Wagner**[4], **Nadeem. A. Vellore**[5], **Christopher A. Eide**[6,7], **Matthew. S. Zabriskie**[5], **Maria. E. Arcila**[8], **Jaclyn F. Hechtman**[8], **Lu Wang**[8], **Roger S. Smith**[3], **Mark. G. Kris**[1,2], **Gregory. J. Riely**[1,2], **Brian. J. Druker**[6,7], **Thomas O'Hare**[5], **Marc. Ladanyi**[3,8], and **Monika. A. Davare**[4,*]

[1]Thoracic Oncology Service, Division of Solid Tumor Oncology, Department of Medicine, Memorial Sloan Kettering Cancer Center, New York, NY 10065, USA

[2]Weill Cornell Medical College, New York, NY 10065, USA

[3]Human Oncology and Pathogenesis Program, Memorial Sloan Kettering Cancer Center, New York, NY 10065, USA

[4]Knight Cancer Institute and Department of Pediatrics, Oregon Health & Science University, Portland, OR 97239, USA

[5]Huntsman Cancer Institute and Division of Hematology and Hematologic Malignancies, The University of Utah, Salt Lake City, UT 84112, USA

[6]Knight Cancer Institute and Division of Hematology and Medical Oncology, Oregon Health & Science University, Portland, OR 97239, USA

[7]Howard Hughes Medical Institute, Portland, OR 97239, USA

[8]Department of Pathology, Memorial Sloan Kettering Cancer Center, New York, NY 10065, USA

Abstract

Purpose—Rearranged ROS1 is a crizotinib-sensitive oncogenic driver in lung cancer. The development of acquired resistance, however, poses a serious clinical challenge. Consequently, experimental and clinical validation of resistance mechanisms and potential second-line therapies is essential.

Experimental Design—We report the discovery of a novel, solvent-front ROS1^{D2033N} mutation in a patient with CD74-ROS1-rearranged lung adenocarcinoma and acquired resistance to

[*]To whom correspondence should be addressed: Alexander Drilon, MD, drilona@mskcc.org, Thoracic Oncology Service, Division of Solid Tumor, Oncology, Department of Medicine, Memorial Sloan Kettering Cancer Center, 300 E 66th St. BAIC 1253, New York, NY 10065, USA, Phone: 646-888-4206 Fax: 646-888-4263, Monika A. Davare, PhD, davarem@ohsu.edu, Knight Cancer Institute & Department of Pediatrics, Oregon Health & Science University, 3181 SW Sam Jackson Park Road, Mailcode L592/BRB553, Portland, OR 97239, USA, Phone: 503-494-3431 Fax: 503-494-3688.

Author contributions: A.D., R.S., N.A.V., C.A.E., T.O., M.L., and M.A.D. contributed to the conception and design of this study. A.D., R.S., J.P.W., N.A.V., C.A.E., M.S.Z., M.A., J.F.H, L.W., R.S., M.G.K., G.J.R., B.J.D., T.O., M.L., and M.A.D. contributed to the acquisition, analysis, or interpretation of the data, and drafting and revision of the manuscript.

Conflict of Interest: A.D. has served as a consultant for Exelixis.

Author Manuscript Author Manuscript Author Manuscript Author Manuscript

crizotinib. Crizotinib-resistance of CD74-ROS1^{D2033N} was functionally evaluated using cell based assays and structural modelling.

Results—In biochemical and cell-based assays, the CD74-ROS1^{D2033N} mutant demonstrated significantly decreased sensitivity to crizotinib. Molecular dynamics simulation revealed compromised crizotinib binding due to drastic changes in the electrostatic interaction between the D2033 residue and crizotinib and reorientation of neighboring residues. In contrast, cabozantinib binding was unaffected by the D2033N substitution and inhibitory potency against the mutant was retained. Notably, cabozantinib treatment resulted in a rapid clinical and near complete radiographic response in this patient.

Conclusions—These results provide the first example of successful therapeutic intervention with targeted therapy to overcome crizotinib resistance in a ROS1-rearranged cancer.

Keywords

ROS1; Targeted Therapy; Lung Cancer; Resistance; Cabozantinib

Introduction

Chromosomal rearrangements of the receptor tyrosine kinase *ROS1* are oncogenic drivers in multiple malignancies (1). Fusion of the intact *ROS1* tyrosine kinase domain with various gene partners results in constitutive activation of downstream pathways responsible for tumor growth and proliferation. In lung adenocarcinomas, ROS1 rearrangements comprise a distinct molecular subset of tumors present in 1–2% of patients. CD74-ROS1 is the most common fusion in this context (2–4).

ROS1-rearranged lung cancers are highly sensitive to treatment with the ROS1/ALK tyrosine kinase inhibitor (TKI) crizotinib (5), with a response rate of 72% and a median progression-free survival of 19 months based on phase 1 expansion cohort data (6). Consistent with the experience with crizotinib in the treatment of advanced ALK-rearranged lung cancers, acquired resistance has also begun to emerge in patients harboring ROS1 fusions (7), although the scope of such resistance mechanisms in this setting remain unknown. Second-generation ROS1 inhibitors are in clinical development and may provide viable treatment options for patients with resistance to crizotinib, but clinical response to these agents has not been published to date.

We report the identification of a novel ROS1 solvent-front mutation in a patient with a CD74-ROS1-rearranged lung adenocarcinoma who developed acquired resistance to crizotinib. Treatment with cabozantinib – an FDA-approved TKI with activity against ROS1 (8) – resulted in rapid clinical and radiographic responses, providing the first example of overcoming crizotinib resistance with oral targeted therapy in a patient with a ROS1-rearranged malignancy. Furthermore, we provide functional validation of and structural insight into the mechanism of resistance to crizotinib and the efficacy of cabozantinib.

Author Manuscript Author Manuscript Author Manuscript Author Manuscript

Materials and Methods

Molecular profiling and next-generation sequencing

Initial screening for a *ROS1* fusion was performed via a dual-probe fluorescence in situ hybridization (FISH) break-apart test. On the basis of an upper level of split signals for break-apart probes (5' green probe and 3' red probe flanking the *ROS1* kinase domain) on normal formalin-fixed paraffin-embedded tissue sections of approximately 5 μm, the cutoff for scoring the *ROS1* FISH assay as positive for the presence of a rearrangement was set at 12% of cells with split signals or isolated 3′ signals. Broad, hybrid-capture next-generation sequencing was performed using the MSK-IMPACT (Integrated Mutational Profiling of Actionable Cancer Targets) Illumina HiSeq 2500 platform (9). A total of 341 cancer-related genes were interrogated, capturing base substitutions, small indels, copy number alterations, and select rearrangements. To detect somatic structural aberrations, a framework was developed that first aligns raw reads to the reference human genome (hg19) using the Burrows-Wheeler Alignment tool. Duplicates are then filtered using the Picard-tools java package (samtools) and searched for candidate structural rearrangements using DELLY. All candidate somatic structural aberrations were filtered, annotated using in-house tools, and manually reviewed using the Integrative Genomics Viewer (IGV).

Cabozantinib administration

The patient received cabozantinib at a dose of 60 mg daily in 28-day cycles as part of an ongoing phase II clinical trial (NCT01639508) with an arm for *ROS1*-rearranged lung cancers. Inclusion criteria for patients in this trial were as follows: pathologic or cytologic evidence of non-small-cell lung cancer (NSCLC), clinical stage IV or recurrent/medically inoperable disease, a Karnofsky performance status of more than 70%, a life expectancy of more than 12 weeks, adequate hematologic, renal, and hepatic function, and measurable disease. Informed consent was obtained after the nature and possible consequences of the studies were explained. Treatment was discontinued in the event of disease progression, unacceptable toxicity, or patient withdrawal. Dose reductions were permitted as per a prescribed algorithm. Response was assessed using the Response Evaluation Criteria in Solid Tumors (RECIST) version 1.1 (10). Imaging was performed at baseline, 4 weeks, and every 8 weeks thereafter. In addition, scans to confirm response were performed as per RECIST. The primary endpoint of the trial was objective response. Secondary endpoints included progression-free survival and overall survival.

Cell culture

Parental Ba/F3 cells (American Type Culture Collection, ATCC) were cultured in complete medium (RPMI medium 1640 with 10% (vol/vol) FBS, L-glutamine, penicillin/streptomycin) supplemented with 15% (vol/vol) WEHI-3-conditioned media as a source of IL-3. CD74-ROS1^{D2033N} was generated using site-directed mutagenesis by following manufacturer's protocol (Agilent). Ba/F3 cells were maintained at densities of 0.5–1.5×10^6 cells/mL and infected with retrovirus encoding native or mutant versions of human CD74-ROS1. GFP-based selection of transduced cells was performed with a FACSAria cell sorter (BD Biosciences). Stable cell lines were washed with complete medium to remove IL-3.

Author Manuscript Author Manuscript Author Manuscript Author Manuscript

Cells that grew out after IL-3 withdrawal were maintained in complete medium and used for *in vitro* assays.

Apoptosis measurement

Ba/F3 cells expressing native CD74-ROS1 or CD74-ROS1^{D2033N} were treated with 1, 10, and 100 nM crizotinib or cabozantinib for 72 h. The Guava Nexin Assay Kit (EMD/Millipore) was used to detect apoptosis according to the manufacturer's protocol. Annexin V-positive cells were counted using a Guava easyCyte flow cytometer (Millipore).

Cell growth/viability assays

Inhibitors were prepared as 1 mM stocks in DMSO prior to each experiment. Inhibitors were distributed at 2X concentration using a D300 Digital Dispenser (Hewlett-Packard) capable of accurately administering very small volumes (10 pL-150 nL) into 384-well plates pre-loaded with 25 μL/well of complete medium. Ba/F3 cells expressing CD74-ROS1 constructs were seeded (800 cells/well; 25 μL) into drug plates using a Multidrop Combi Reagent Dispenser (Thermo Scientific), and plates were incubated for 72 h at 37°C, 5% CO2. Viability was measured using a methanethiosulfonate (MTS)-based assay (CellTiter96 Aqueous One Solution; Promega) read on a Biotek Synergy 2 plate reader. Proliferation experiments were performed three independent times in triplicate. Data were normalized using Microsoft Excel, and 50% and 90% growth inhibitory concentration (IC_{50} and IC_{90}) values were calculated with GraphPad Prism software using a non-linear curve fit equation modified using previously described parameters (11).

Immunoblot analysis

Ba/F3 CD74-ROS1 and CD74-ROS1^{D2033N} cells were treated with the indicated concentrations of inhibitors for 2 h, pelleted, washed once in ice-cold PBS, and lysed in 200 μL of cell lysis buffer (Cell Signaling Technology) that was supplemented with 0.25% deoxycholate, 0.05% SDS, and protease and phosphatase inhibitors. Equal amounts of protein were extracted with SDS sample buffer for 15 min at 80°C and resolved on 4–15% Tris-glycine or 4–12% Bis-Tris precast gels (Criterion; Bio-Rad). Proteins transferred to Immobilon-FL membranes (Millipore) were probed with: phospho-ROS1 [Cell Signaling Technology (CST); 3078, 1:1000], total ROS1 (CST; 3266, 1:1000), phospho-ERK1/2 (CST; 9101, 1:1000), total ERK2 (Santa Cruz; sc-1647, 1:2000), phospho-AKT (CST; 4060, 1:1000), AKT (BD Transduction Laboratories; 610860, 1:1000), pSHP2 (CST; 3703), pSTAT3 (CST, 9131), and GAPDH (Ambion; AM4300, 1:5000). Blots were imaged using either a LI-COR Odyssey imaging system or the Bio-Rad ChemiDoc imaging station according to the manufacturer's protocol for immunoblot detection with use of Infrared dye or horseradish peroxidase-conjugated secondary antibodies, respectively.

Molecular models of native ROS1 and ROS1^{D2033N}

The crystal structure of the active conformation of the ROS1 kinase domain in complex with crizotinib was used for structural studies (PDB entry 3ZBF) (7); however, missing residues in the P-loop and A-loop were modeled using Schrödinger Suite (version 3.1; Schrödinger, LLC) and hydrogen atoms were added. The ROS1^{D2033N} structure was generated using the

Author Manuscript Author Manuscript Author Manuscript Author Manuscript

native ROS1 crystal structure, by single amino-acid substitution. In the absence of a crystal structure for the inactive conformation of ROS1 kinase, a homology-based model was generated. Using the Prime module of Schrödinger's package, a knowledge-based model was built for both native ROS1 and ROS1^{D2033N}. The crystal structure of ALK (PDB entry 4FNY) (12) in the inactive state was used as a structural template (sequence homology ~64%) to build inactive ROS1. All four systems (ROS1 and ROS1^{D2033N} in both the active and inactive states) were solvated using a pre-equilibrated TIP3P water-box (13), maintaining a distance of 20 Å from any protein atom to the edge of the box. Compatible sodium and chloride ions were added to neutralize the simulated systems (14). The final orthorhombic box contained a total of 68,758–72,236 atoms.

Ensemble docking

Ensemble docking was performed using the Glide program of Schrödinger's package (Suite 2012: Maestro, version 9.3). 500 conformations were extracted from each system simulated (one conformation for every nanosecond) and a docking grid for the receptor was generated using the binding site residues (L1951, A1978, K1980, E1997, M2001, L2028, G2032, L2086, and D2102). Ligands (crizotinib and cabozantinib) were prepared using the Ligprep module of the Schrödinger's package (version 3), docked using the GlideXP method (Glide version 5.8; Schrödinger, LLC), and analyzed for binding interactions (15). The most favorable docking score computed using the ensemble docking was reported.

Molecular dynamics simulations

Molecular dynamics (MD) simulations were performed using the Amber ff12SB force field (16) in the NAMD simulation software (17). All hydrogen atoms were restrained using the SHAKE algorithm (18). Periodic boundary conditions with particle mesh Ewald (PME) summation were employed to handle the long-range electrostatic interactions (real-space truncation at 9.0 Å and grid spacing of 1.0 Å) (19). Temperature and pressure were controlled at 300 K and 1 atm using the Nose'-Hoover Langevin piston algorithm (20) and Langevin dynamics (21), respectively. All four systems were simulated for 500 ns and coordinates were saved every 10 ps for further conformational analysis. The CPPTRAJ software of the AmberTools suite was used for post-processing of the MD generated trajectories (22). Electrostatic potential surface representation of native ROS1 and ROS1^{D2033N} was generated using Adaptive Poisson-Boltzmann Software (23).

Results

Discovery of the ROS1 D2033N mutation and response to cabozantinib in the setting of acquired resistance to crizotinib

A 50 year-old female never smoker with metastatic lung adenocarcinoma involving the pleura received three cycles of first-line systemic therapy with cisplatin, pemetrexed, and bevacizumab (Fig. 1, Supplementary Table S1). Rearrangement of *ROS1* was detected via fluorescence in situ hybridization (FISH) and confirmed by sequencing using MSK-IMPACT, a validated broad, hybrid-capture next-generation sequencing (NGS) test (9), as an in-frame fusion of *CD74* (exons 1–6) with *ROS1* (exons 34–42) in the diagnostic biopsy sample. The patient was treated with crizotinib (250 mg twice daily), achieving a durable

Author Manuscript Author Manuscript Author Manuscript Author Manuscript

partial response (64% reduction in disease burden via RECIST v1.1 (10)). At 18 months, she underwent whole brain radiation for new brain metastases. Disease control outside the brain was maintained on crizotinib.

After a total of 26 months on crizotinib, the patient developed widespread disease progression. Computed and positron emission tomography (CT/PET) identified new bilateral pulmonary nodules, mediastinal and retroperitoneal adenopathy, and peritoneal carcinomatosis (Fig. 2, left panel). To identify molecular mechanism(s) of crizotinib-resistance, we analyzed a biopsy from a growing retroperitoneal lymph node after progression on crizotinib using NGS that confirmed persistent expression of the *CD74-ROS1* rearrangement (Fig. 1 and Supplementary Fig. S1A). This deep-sequencing also revealed the acquisition of a novel mutation, *ROS1* D2033N (c.6097G>A), that resides within the ROS1 kinase domain (Fig. 1 and Supplementary Fig. S1B) and was not detected in the pre-crizotinib diagnostic sample from this patient (Supplementary Fig. S1A).

Of 644 sequencing reads over that specific region of ROS1 that were at 663X depth, the variant frequency of c.6097G>A was 14% in the crizotinib-resistant tumor specimen and undetectable the matched normal peripheral blood control. Additional morphologic assessment of tumor content as well as FISH analysis shows that the tumor content was 60–70% and the *CD74-ROS1* fusion was identified in 70% of the cells analyzed. This suggests that the acquired D2033N mutation is subclonal and present in about 20–23% of the tumor cells that harbor the CD74-ROS1 fusions. While these data strongly suggest that ROS1^{D2033N} is a novel acquired crizotinib-resistant mutation, we cannot rule out the possibility that a very rare population (frequency < 2%) was present in the pre-crizotinib treatment sample that was below the detection threshold of NGS platform used here. Given clinical resistance to crizotinib, the ROS1 inhibitor cabozantinib was initiated (60 mg daily) on a phase II clinical trial (NCT01639508). Partial response was rapidly achieved by 4 weeks, and confirmed at 8 weeks (Fig. 2, right panel). At 12 weeks, a near complete response was achieved with a 92% reduction in disease burden. The patient remains on therapy approaching 8 months (Fig. 1).

Functional assessment of crizotinib and cabozantinib sensitivity against the CD74-ROS1^{D2033N} mutant in cell-based assays

To assess the role of the CD74-ROS1^{D2033N} mutation as a causative mechanism for crizotinib-resistance, we performed cell-based sensitivity profiling using Ba/F3 cells transformed with native CD74-ROS1 or CD74-ROS1^{D2033N} (Supplementary Fig. 2A). Ba/F3 cells are an interleukin-3-dependent pro-B murine cell line that is a well-established model system for eliciting oncogene addiction and testing kinase inhibitor efficacy (24). During interleukin-3 withdrawal of Ba/F3 cells, CD74-ROS1 and CD74-ROS1^{D2033N} conferred comparable capacity for and kinetics of outgrowth in the absence of the requisite cytokine, suggesting that the mutation does not provide a fitness or growth advantage (Supplementary Fig. 2A). However, while crizotinib exhibited markedly reduced growth inhibition of Ba/F3 CD74-ROS1^{D2033N} cells as compared to native CD74-ROS1 cells (IC_{50}: 132.3 versus 21.4 nM, respectively; Fig. 3A), cabozantinib potently inhibited the growth of both native and D2033N-mutant CD74-ROS1 cells (IC_{50}: 0.78 versus 2.8 nM, respectively).

Author Manuscript Author Manuscript Author Manuscript Author Manuscript

Inhibition of Ba/F3 CD74-ROS1^{D2033N} cells by cabozantinib was consistent with induction of apoptotic cell death (Supplementary Fig. S2B). Immunoblot assessment following short-term treatment of native CD74-ROS1 cells with crizotinib or cabozantinib showed dose-dependent inhibition of phosphorylation of ROS1 and its downstream effectors SHP2, ERK1/2, AKT and STAT3 (Fig. 3B). However, in CD74-ROS1^{D2033N} cells, only treatment with cabozantinib suppressed ROS1 activation and downstream signaling (Fig. 3B). To characterize the spectrum of inhibitor sensitivity of CD74-ROS1^{D2033N}, we also evaluated the sensitivity of this mutant to a panel of other ROS1 kinase inhibitors at varying stages of clinical development (Supplementary Fig. S3A–D). As compared to cells expressing native CD74-ROS1, the CD74-ROS1^{D2033N} mutant conferred 4.3-, 3.7- and 7-fold decrease in sensitivity to ceritinib, brigatinib, and PF-06463922, respectively, but remained highly sensitive to foretinib, a close structural analog of cabozantinib (Supplementary Fig. S3E & F). Furthermore, although the sensitivity of CD74-ROS1^{D2033N} to PF-06463922 was reduced seven-fold, due to high potency of this recently described heterocyclic ROS1 inhibitor (Supplementary Fig. S3B & E) (25), the CD74-ROS1^{D2033N} mutant is still inhibited in the low nanomolar range *in vitro*.

Structural differences in the binding requirements of crizotinib and cabozantinib underlie inhibitor resistance versus sensitivity

To further understand the resistance and selectivity imparted by the D2033N mutation, we performed molecular dynamics (MD) simulation of the native and mutant ROS1 kinase domains using the available X-ray crystal structure (7) and docking analysis of inhibitors on the MD-generated ensemble (Fig. 4A). Both the native ROS1 and ROS1^{D2033N} systems were stable during the 500 ns MD simulation and displayed a similar conformation of the ATP-binding site. ROS1^{D2033N} showed slight reduction in the flexibility of the P-loop compared to native ROS1, possibly due to re-orienting of the carbonyl moiety of P-loop residue L1951, which is necessary to participate in a water-mediated hydrogen bond with N2033.

More dramatically, the D2033N mutation dictates a major change in the electrostatic potential at the exterior surface of the ATP-binding site. Docking analysis performed on the native ROS1 ensemble revealed a strong electrostatic interaction between the protonated piperidine moiety of crizotinib and the negatively charged D2033 residue (Fig. 4B, top panel). This key interaction is lost as a result of the D2033N mutation, which lacks the negatively charged functional group optimally positioned to interact with this region of bound crizotinib. This mutation also induced subtle reorientations of neighboring residues that further hindered favorable interaction with the protonated piperidine region of crizotinib.

Hypothetical placement of crizotinib on the ROS1^{D2033N} mutant (based on structural alignment) indicated electrostatic repulsion between the positively charged piperidine nitrogen and the amine group of N2033 (Fig. 4B, middle panel). In contrast, the nearest portion of the cabozantinib binding site was at least 5 Å away from residue 2033 in both native ROS1 and ROS1^{D2033N}, and its binding does not involve interaction with this residue in either case (Fig. 4B, bottom panel). Consistently, comparatively poorer docking scores

Author Manuscript Author Manuscript Author Manuscript Author Manuscript

were observed for crizotinib for the ROS1^{D2033N} mutant versus native ROS1 (−7 kcal/mol and −9.6 kcal/mol, respectively; lower scores indicate stronger inhibitor binding), whereas favorable and comparable docking scores were seen for cabozantinib bound to ROS1^{D2033N} and native ROS1 (−10 and −12 kcal/mol, respectively).

Homology alignment suggests that the native aspartate at position 2033 of ROS1 is highly conserved among ROS1 paralogs, although significant variability is seen among other less closely related kinases (Fig. 4C). Interestingly, the analogous position in ABL1 kinase (322) is an asparagine, thus phylogenetically mimicking the ROS1^{D2033N} mutation. Although structural modeling shows similarity in the active conformations of the ROS1 and ABL1 kinase domains, docking simulations suggest that the lack of productive electrostatic interaction may contribute to crizotinib's selectivity for ROS1 over ABL1 (26) (Fig. 4D).

Discussion

We have identified ROS1^{D2033N} as a novel mechanism of acquired resistance to crizotinib therapy in ROS1-rearranged lung cancer. The D2033N mutation occurs at the solvent-front region of the ATP-binding site of ROS1, similar to G2032R, the only other acquired resistance mutation that has been identified in a patient to date (7, 27). As follow-up of ROS1-rearranged lung cancer patients treated with crizotinib is still relatively short, subsequent sequencing analysis of larger cohorts of crizotinib-resistant patients will be required to better establish the spectrum and frequency of mutations such as D2033N. The analogous mutation in the highly related ALK kinase (D1203N) has not been reported in clinical crizotinib resistance in *ALK*-rearranged lung cancer, but it was detected in a cell-based *in vitro* screen for resistance to crizotinib (28). While second-generation ROS1 inhibitors are effective *in vitro* against select ROS1 kinase domain mutations identified from cell-based resistance screens, including those at the gatekeeper position, mutations arising in the solvent-front region are resistant to several of these agents (8). Identifying ROS1 inhibitors that are active in this setting is thus crucial, and as shown here, can have a substantial impact on clinical outcome.

This mutation confers high-level resistance to crizotinib *in vitro*, compromising drug binding secondary to a major change in electrostatic interaction and reorientation of neighboring residues. We demonstrate that cabozantinib overcomes acquired resistance to crizotinib mediated by the ROS1^{D2033N} mutation, inducing downstream pathway inhibition and apoptotic cell death. While in vitro characterization suggests a potentially slightly increased sensitivity of the D2033N mutant to cabozantinib relative to native CD74-ROS1, expanded structural studies would be required to interrogate such subtle changes in IC_{50}. Structural modeling suggests accommodation of this mutation by cabozantinib, corroborating previous data showing that cabozantinib is likewise active against the ROS1^{G2032R} mutant (8, 29) and, implies a broader role for this compound in circumventing crizotinib-resistant solvent-front mutations.

While the CD74-ROS1^{D2033N} mutation was detected as subclonal population in the patient under study, the rapid and near complete tumor response to the more potent ROS1 inhibitor cabozantinib (92% reduction in 12 weeks) combined with *in vitro* cell-based and structural

Author Manuscript Author Manuscript Author Manuscript Author Manuscript

validation experiments strongly implicate it as the dominant mechanism of crizotinib-resistance in this patient. The evidence for clinical resistance in the setting of only a subclonal resistant cell population is not surprising, as a similar scenario is common, for example, to the development of the well-characterized secondary $EGFR^{T790M}$ resistance mutation in non-small cell lung carcinoma patients harboring a sensitizing mutation and treated with EGFR inhibitors (30, 31). These mutations are often found in only small proportion of the tumor cells, yet result in profound acquired resistance in patients.

Importantly, this report represents the first clinical description of a dramatic response to ROS1-directed targeted therapy in the setting of acquired resistance to crizotinib. Pre-clinical validation experiments strongly suggest that the dramatic clinical response to cabozantinib is due to potent inhibitory activity against the acquired CD74-$ROS1^{D2033N}$ mutation; however, we cannot formally rule out potential additive or synergistic effects that may result from inhibiting the primary driver ROS1 along with other target(s) of cabozantinib (VEGFR2 and AXL) that regulate angiogenesis. These findings highlight the growing need to further characterize mechanisms of acquired resistance to ROS1 TKI therapy in a systematic fashion, at the level of structural and functional validation as well as in the clinic. Many of these studies are ongoing and are likely to inform clinical practice in the future. Whenever possible, we recommend that comprehensive molecular profiling be performed for all patients in the setting of acquired resistance to guide appropriate therapy selection. A prospective phase 2 trial of cabozantinib with a cohort for ROS1-rearranged lung cancer continues to enroll patients (NCT01639508).

Supplementary Material

Refer to Web version on PubMed Central for supplementary material.

Acknowledgments

No specific acknowledgements.

Financial Support: This work was partly supported by NIH grant P01CA12943 (M.L., M.G.K., L.W.). The MSK-IMPACT program is supported in part by the Marie-Josée and Henry R. Kravis Center for Molecular Oncology. M.A.D. is supported by the Hyundai Scholar Hope grant. T.O. is supported by the NIH (R01 CA178397-01). B.J.D. is an investigator for the Howard Hughes Medical Institute.

References

1. Davare MA, Tognon CE. Detecting and targeting oncogenic fusion proteins in the genomic era. Biol Cell. 2015
2. Rimkunas VM, Crosby KE, Li D, Hu Y, Kelly ME, Gu TL, et al. Analysis of receptor tyrosine kinase ROS1-positive tumors in non-small cell lung cancer: identification of a FIG-ROS1 fusion. Clin Cancer Res. 2012; 18:4449–4457. [PubMed: 22661537]
3. Takeuchi K, Soda M, Togashi Y, Suzuki R, Sakata S, Hatano S, et al. RET, ROS1 and ALK fusions in lung cancer. Nat Med. 2012; 18:378–381. [PubMed: 22327623]
4. Bergethon K, Shaw AT, Ou SH, Katayama R, Lovly CM, McDonald NT, et al. ROS1 rearrangements define a unique molecular class of lung cancers. J Clin Oncol. 2012; 30:863–870. [PubMed: 22215748]

Author Manuscript Author Manuscript Author Manuscript Author Manuscript

5. Mazieres J, Zalcman G, Crino L, Biondani P, Barlesi F, Filleron T, et al. Crizotinib Therapy for Advanced Lung Adenocarcinoma and a ROS1 Rearrangement: Results From the EUROS1 Cohort. J Clin Oncol. 2015; 33:992–999. [PubMed: 25667280]
6. Shaw AT, Ou SH, Bang YJ, Camidge DR, Solomon BJ, Salgia R, et al. Crizotinib in ROS1-rearranged non-small-cell lung cancer. N Engl J Med. 2014; 371:1963–1971. [PubMed: 25264305]
7. Awad MM, Katayama R, McTigue M, Liu W, Deng YL, Brooun A, et al. Acquired resistance to crizotinib from a mutation in CD74-ROS1. N Engl J Med. 2013; 368:2395–2401. [PubMed: 23724914]
8. Katayama R, Kobayashi Y, Friboulet L, Lockerman EL, Koike S, Shaw AT, et al. Cabozantinib overcomes crizotinib resistance in ROS1 fusion-positive cancer. Clin Cancer Res. 2015; 21:166–174. [PubMed: 25351743]
9. Cheng DT, Mitchell TN, Zehir A, Shah RH, Benayed R, Syed A, et al. Memorial Sloan Kettering-Integrated Mutation Profiling of Actionable Cancer Targets (MSK-IMPACT): A Hybridization Capture-Based Next-Generation Sequencing Clinical Assay for Solid Tumor Molecular Oncology. J Mol Diagn. 2015; 17:251–264. [PubMed: 25801821]
10. Eisenhauer EA, Therasse P, Bogaerts J, Schwartz LH, Sargent D, Ford R, et al. New response evaluation criteria in solid tumours: revised RECIST guideline (version 1.1). Eur J Cancer. 2009; 45:228–247. [PubMed: 19097774]
11. Sebaugh JL. Guidelines for accurate EC50/IC50 estimation. Pharm Stat. 2011; 10:128–134. [PubMed: 22328315]
12. Epstein LF, Chen H, Emkey R, Whittington DA. The R1275Q neuroblastoma mutant and certain ATP-competitive inhibitors stabilize alternative activation loop conformations of anaplastic lymphoma kinase. J Biol Chem. 2012; 287:37447–37457. [PubMed: 22932897]
13. Jorgensen WLCJ, Madura JD, Impey RW, Klein ML. Comparison of simple potential functions for simulating liquid water. J Chem Phys. 1983; 79
14. Joung IS, Cheatham TE 3rd. Determination of alkali and halide monovalent ion parameters for use in explicitly solvated biomolecular simulations. J Phys Chem B. 2008; 112:9020–9041. [PubMed: 18593145]
15. Friesner RA, Murphy RB, Repasky MP, Frye LL, Greenwood JR, Halgren TA, et al. Extra precision glide: docking and scoring incorporating a model of hydrophobic enclosure for protein-ligand complexes. J Med Chem. 2006; 49:6177–6196. [PubMed: 17034125]
16. Case, DA. AMBER 12. San Fransisco: University of California; 2012.
17. Phillips JC, Braun R, Wang W, Gumbart J, Tajkhorshid E, Villa E, et al. Scalable molecular dynamics with NAMD. J Comput Chem. 2005; 26:1781–1802. [PubMed: 16222654]
18. Miyamoto S, Kollman PA. Settle: An analytical version of the SHAKE and RATTLE algorithm for rigid water models. J Comput Chem. 1992; 13:952–962.
19. Darden T, York D, Pedersen L. Particle mesh Ewald: An N · log(N) method for Ewald sums in large systems. J Chem Phys. 1993; 98:10089.
20. Martyna GJ, Tobias DJ, Klein ML. Constant pressure molecular dynamics algorithms. J Chem Phys. 1994; 101:4177.
21. Pastor RW, Brooks BR, Szabo A. An analysis of the accuracy of Langevin and molecular dynamics algorithms. Mol Phys. 1988; 65:1409–1419.
22. Roe DR, Cheatham TE. PTRAJ and CPPTRAJ: Software for Processing and Analysis of Molecular Dynamics Trajectory Data. J Chem Theory Comput. 2013; 9:3084–3095. [PubMed: 26583988]
23. Baker NA, Sept D, Joseph S, Holst MJ, McCammon JA. Electrostatics of nanosystems: application to microtubules and the ribosome. Proc Natl Acad Sci U S A. 2001; 98:10037–10041. [PubMed: 11517324]
24. Warmuth M, Kim S, Gu XJ, Xia G, Adrian F. Ba/F3 cells and their use in kinase drug discovery. Curr Opin Oncol. 2007; 19:55–60. [PubMed: 17133113]
25. Zou HY, Li Q, Engstrom LD, West M, Appleman V, Wong KA, et al. PF-06463922 is a potent and selective next-generation ROS1/ALK inhibitor capable of blocking crizotinib-resistant ROS1 mutations. Proc Natl Acad Sci U S A. 2015; 112:3493–3498. [PubMed: 25733882]

Author Manuscript Author Manuscript Author Manuscript Author Manuscript

26. Cui JJ, Tran-Dube M, Shen H, Nambu M, Kung PP, Pairish M, et al. Structure based drug design of crizotinib (PF-02341066), a potent and selective dual inhibitor of mesenchymal-epithelial transition factor (c-MET) kinase and anaplastic lymphoma kinase (ALK). J Med Chem. 2011; 54:6342–6363. [PubMed: 21812414]

27. Song A, Kim TM, Kim DW, Kim S, Keam B, Lee SH, et al. Molecular changes associated with acquired resistance to crizotinib in ROS1-rearranged non-small cell lung cancer (NSCLC). Clin Cancer Res. 2015

28. Heuckmann JM, Holzel M, Sos ML, Heynck S, Balke-Want H, Koker M, et al. ALK mutations conferring differential resistance to structurally diverse ALK inhibitors. Clin Cancer Res. 2011; 17:7394–7401. [PubMed: 21948233]

29. Davare MA, Vellore NA, Wagner JP, Eide CA, Goodman JR, Drilon A, et al. Structural insight into selectivity and resistance profiles of ROS1 tyrosine kinase inhibitors. Proc Natl Acad Sci U S A. 2015; 112:E5381–E5390. [PubMed: 26372962]

30. Ohashi K, Maruvka YE, Michor F, Pao W. Epidermal growth factor receptor tyrosine kinase inhibitor-resistant disease. J Clin Oncol. 2013; 31:1070–1080. [PubMed: 23401451]

31. Ladanyi M, Pao W. Lung adenocarcinoma: guiding EGFR-targeted therapy and beyond. Mod Pathol. 2008; 21(Suppl 2):S16–S22. [PubMed: 18437168]

Author Manuscript Author Manuscript Author Manuscript Author Manuscript

Statement of Translational Relevance

The emergence of resistance to targeted therapy is a recurrent clinical challenge and requires development and validation of secondary agents with improved activity. Accompanied by experimental cell-based and structural validation, this report of a near complete response to cabozantinib in a ROS1-rearranged lung adenocarcinoma patient with acquired resistance to crizotinib mediated by a novel CD74-ROS1^{D2033N} solvent-front mutation provides the first clinical example of crizotinib resistance overcome by targeted therapy in a ROS1-rearranged malignancy.

Author Manuscript Author Manuscript Author Manuscript Author Manuscript

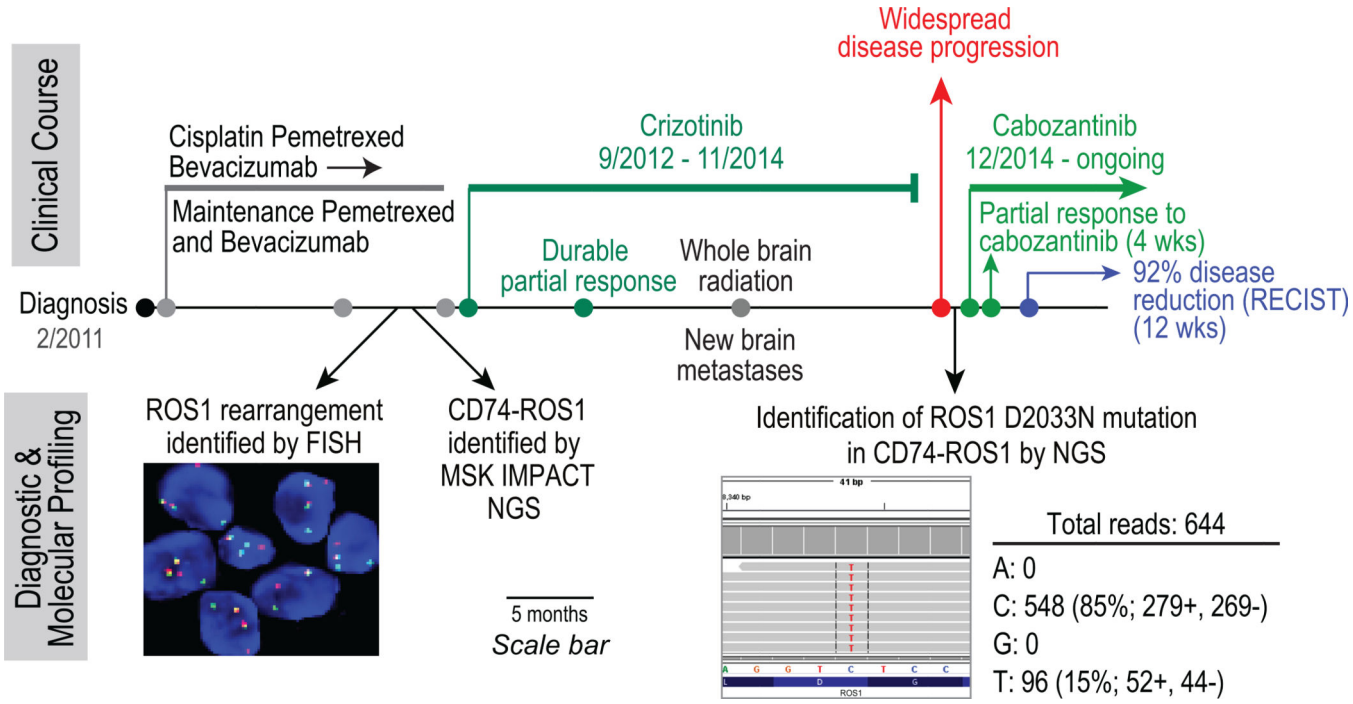

Figure. 1. A patient with *CD74-ROS1*-rearranged lung adenocarcinoma and acquired resistance to crizotinib mediated by a novel CD74-ROS1^{D2033N} mutation responds to therapy with cabozantinib

The patient's clinical course and treatment history are depicted chronologically moving left to right. Rearranged *ROS1* was initially detected via break-apart FISH assay. Split green (5' probe) and red (3' probe) signals indicate the presence of a *ROS1* fusion, subsequently identified as *CD74-ROS1*. Broad, hybrid-capture next-generation sequencing of pre- and post-crizotinib tumor detected an acquired c.6097G>A (D2033N) mutation within the *ROS1* kinase domain at the time of disease progression. A partial response to cabozantinib (RECIST v1.1) was achieved and confirmed at 8 weeks. This was accompanied by a clinical response to therapy (substantial improvement in cough and abdominal discomfort) noted within a few days of cabozantinib initiation. At 12 weeks, a near complete response was noted with a 92% reduction in disease burden.

Author Manuscript Author Manuscript Author Manuscript Author Manuscript

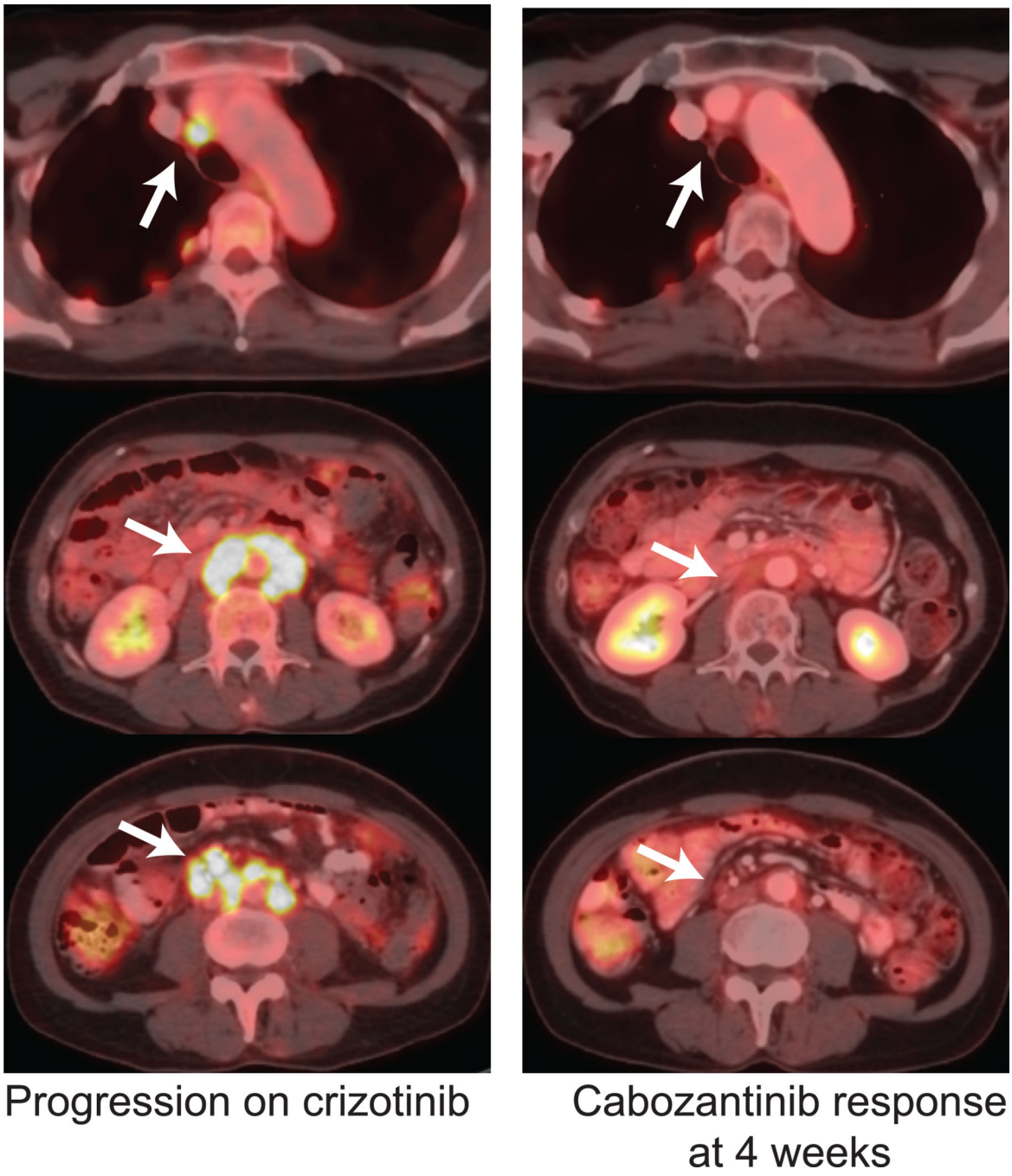

Figure 2. Radiographic evidence of clinical response to cabozantinib

Left panel: Fused CT/PET images demonstrating disease progression at the onset of acquired resistance to crizotinib and prior to cabozantinib treatment. Growing hypermetabolic mediastinal and retroperitoneal adenopathy are indicated by white arrows. *Right panel:* Fused CT/PET images obtained 4 weeks after the initiation of cabozantinib showing rapid resolution of hypermetabolic mediastinal and abdominopelvic lymph nodes.

Author Manuscript Author Manuscript Author Manuscript Author Manuscript

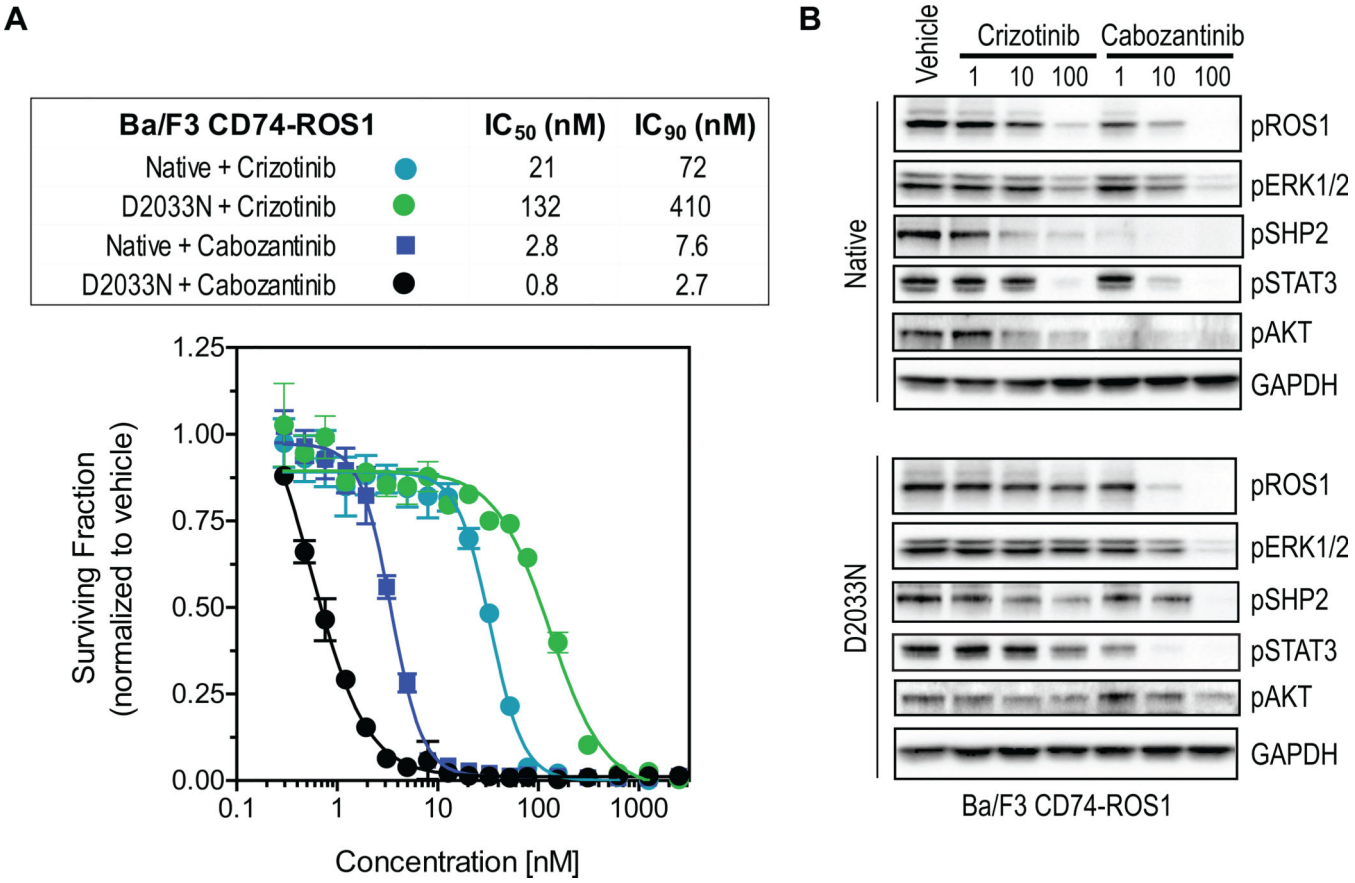

Figure. 3. The CD74-ROS1^{D2033N} mutation confers crizotinib resistance but remains sensitive to cabozantinib

A. Cell growth and viability of Ba/F3 cells expressing native CD74-ROS1 or CD74-ROS1^{D2033N} after 72 h exposure to crizotinib and cabozantinib. Results are shown as mean viability normalized to vehicle-treated control ± SEM (n = 4). Concentrations that decreased cell viability by 50 or 90% are listed as IC_{50} and IC_{90}, respectively. **B**. Immunoblot analysis of ROS1, ERK1/2, SHP2, STAT3 and AKT phosphorylation from Ba/F3 CD74-ROS1 and CD74-ROS1^{D2033N} cells after treatment with the indicated concentrations of crizotinib and cabozantinib. GAPDH expression is included as a loading control.

Author Manuscript Author Manuscript Author Manuscript Author Manuscript

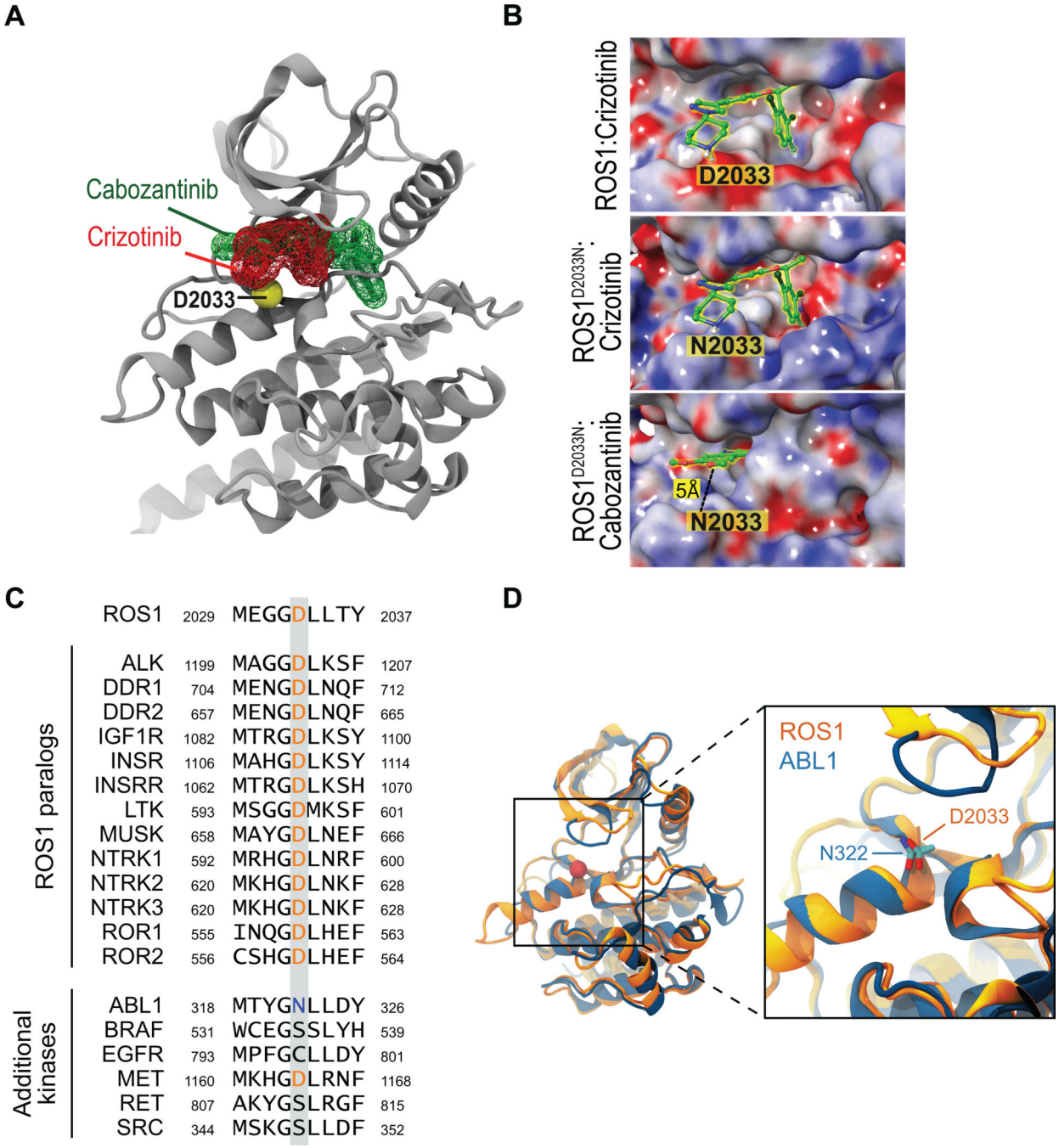

Figure 4. Structural differences in the binding requirements of crizotinib and cabozantinib underlie inhibitor resistance versus sensitivity

A. Structure of the native ROS1 kinase shown as a cartoon model. Crizotinib (red) and cabozantinib (green) binding regions are highlighted using mesh surfaces and residue D2033 is shown as a yellow sphere. **B**. Surface representation of inhibitor docking to native and mutant ROS1. Surfaces are colored according to electrostatic potential (negatively charged region as red and positively charged region as blue). The position and identity of residue 2033 is highlighted, and the indicated inhibitor is shown using a licorice model (green). *Top*

Author Manuscript Author Manuscript Author Manuscript Author Manuscript

panel: Crizotinib bound to native ROS1. *Middle panel*: Hypothetical model of crizotinib binding to $ROS1^{D2033N}$ based on protein alignment. *Bottom panel*: Cabozantinib bound to $ROS1^{D2033N}$ based on docking simulations. **C**. Protein alignment of human ROS1 paralogs and select additional kinases implicated in cancer. A focused window surrounding position 2033 of ROS1 is shown with the analogous position and identity indicated for each protein. **D**. Structural alignment of the active conformations of the ROS1 and ABL1 kinase domains. The crystal structures of active ROS1 and ABL1 are show superimposed in cartoon ribbon format. Position D2033 in ROS1 (red ball) and the analogous position in ABL1 (N322; blue ball) are highlighted for reference.